

An autonomous swarm of micro flying robots with range-based relative localization

Shushuai Li, Mario Coppola, Christophe De Wagter and Guido C. H. E. de Croon

Abstract—Accurate relative localization is an important requirement for a swarm of robots, especially when performing a cooperative task. This paper presents an autonomous multi-robot system equipped with a fully onboard range-based relative positioning system. It uses onboard sensing of velocity, yaw rate, and height as inputs, and then estimates the relative position of other robots in its own body frame by fusing these quantities with ranging measurements obtained from onboard ultra wide-band (UWB) antennas. Simulations concisely show the high precision, efficiency, and stability of the proposed localization method. Experiments are conducted on a team of 5 Crazyflie 2.0 quadrotors, demonstrating autonomous formation flight and pattern formation, and coordinated flight through a window. All results indicate the effectiveness of the proposed relative positioning method for multi-robot systems.

I. INTRODUCTION

Aerial multi-robot systems have been widely studied recently because of their advantages, such as: efficiency of parallel task processing [1], cooperative ability of performing team missions [2], [3], and the ability of smaller drones to operate safely in confined spaces and near humans [4], [5]. These systems require the relative position of peer robots so as to enable intra-swarm collision avoidance, coordination, and more. Therefore, the development of accurate relative localization technologies is an important challenge to be solved.

One solution to the above is to use external positioning systems. For example, there are many indoor examples of teams of multiple quadrotors which are localized with a motion capture system [1], [6], [7]. In [8], 30 drones exhibit outdoor flocking behaviour by relying on a Global Navigation Satellite System (GNSS) for positioning. Alternatively, fixed wireless UWB beacons are another external system that can provide positions for multiple robots [9]. All these systems have been instrumental in illustrating the potential of drone swarms, of how they can pass through a window together [6] or how they can perform beautiful choreographies [7]. However, the availability of aforementioned systems is too limited to allow for autonomous flight in unknown indoor environments. This is due to the poor mobility of the motion capture system, the indoor loss of satellite signals, and the limited coverage area for beacon system.

Other techniques allow for onboard relative localization between multiple robots. Several implementations are based on vision. To simplify the task, [10] and [11] designed a simple pattern that could be detected by a monocular

camera to calculate the relative position of other vehicles. In [3], a follower tracks an April Tag mounted on the leader, enabling the duo to perform a collaborative task. Markerless detection has been explored in [12] with the use of depth images. Vision-based methods have intrinsic scalability, i.e., no limitation on the number of robots. However, these vision based methods are sensitive to the visibility of the markers, which depends on aspects such as the size of the marker and the field of view of the robots' cameras. Another vision-based strategy is not to have the robots detect and localize each other, but to perform a formation flight based on visual inertial odometry [13]. However, this system requires a known initial position of each drone, and can drift over time, potentially leading to losing formation or even collisions.

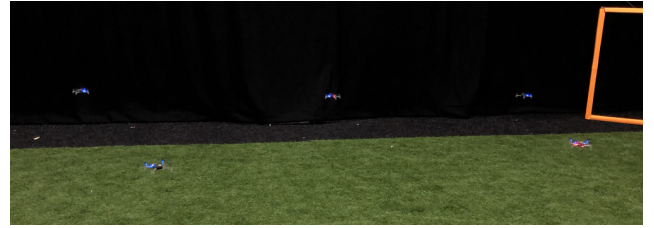


Fig. 1. The autonomous flight of multiple Crazyflie2 quadrotors without GPS or motion capture system, fully based on relative localization using onboard sensing information of velocity, yaw rate, height and ranging measurements between any two robots. Experimental videos can be found in https://www.youtube.com/playlist?list=PL_KSX9GOn2P9sgaX3DHnPsBCJ76fLNJ5.

As an alternative approach, relative localization based on wireless communication between drones has the advantages of being light-weight and omni-directional. Here, the robots use antennas to exchange sensory information (e.g., velocity, yaw rate, height) and combine these with relative range measurements obtained from the antennas. This method was explored by [14] and [15], [16] for aerial robots. These studies required the knowledge of a common orientation. This limitation was overcome in [17], demonstrating a system of 3 drones in leader-follower flight. However, the work of [17] did not deal with the filter's initialization. Additionally, the system can be improved by a faster communication protocol to enhance the update speed, especially in larger teams. This work builds on the previous work of our group on range-based relative localization [14], [17]. We introduce an autonomous multi-robot localization method with faster ranging and communication, and with an autonomous initialization maneuver, and an implementation on off-the-shelf Crazyflie 2.0 quadrotors.

The novel contribution of this article is to improve

wireless-ranging-based relative localization and implement on multiple micro aerial robots to perform different autonomous coordinated tasks. The method does not require any external knowledge or a priori known set-up, such as the knowledge of relative initial positions between drones, as in prior work. Each drone takes the velocity, yaw rate, and height as communicated by the other drones and fuses this information with UWB ranging measurements to get accurate relative locations of peer robots. This work has the following specific contributions: 1) accurate relative localization between multiple micro flying robots with fully onboard perception; 2) an efficient autonomous initialization procedure (due to the lack of knowledge of relative initial positions) based on randomized flight maneuvers; 3) the use of open-source code and commercial robots that can be accessed directly by others for multi-robot applications.

II. PRELIMINARIES

A. Sensory Inputs and Communication

Before introducing the system model, we define the on-board sensing data. For each aerial robot, the 2-axis velocity $\bar{v} = [\bar{v}^x, \bar{v}^y]^T$ in the body frame can be obtained by fusing IMU, height, and optical flow measurements [18]. The yaw rate \bar{r} in the body frame is provided by gyroscope. The range d_{ij} , meaning the distance between robots i and j , can be measured by ultra wide-band sensors. The height h is measured by a downward laser ranger.

Fig. 2. Diagram of relative robot system, composed by two robots shown in a horizontal plane. This frame has a vertical Z-axis and horizontal XY axes, showing the relative 2D position $[x_{ij}, y_{ij}]$ and relative yaw ψ_{ij} of j^{th} robot in i^{th} robot horizontal frame.

\bar{v} and yaw rate \bar{r} need to be transformed before use. The 2-axis velocity $\mathbf{v} = [v^x, v^y]^T$ in horizontal frame can be obtained based on the rotation matrix in X-Y rotation sequence, shown as follows:

where $s(\cdot)$ and $c(\cdot)$ denote $\sin(\cdot)$ and $\cos(\cdot)$, respectively. θ and ϕ are the pitch and roll attitude of each robot obtained from the IMU. In addition, according to the relationship between angular velocity vector and angular velocity, the yaw rate r in horizontal frame can be calculated with the 3-axis gyroscope as follows:

in which \bar{p} and \bar{r} are two axis angular velocity in body frame read from the gyroscope. Since attitude angles are not very large in common real-world, the body-frame yaw rate can be used directly.

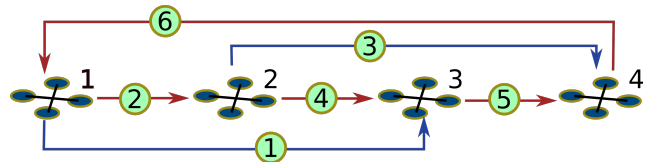


Fig. 3. Communication scheme for multiple robots in an indefinite loop. The communication example pertains to 4 robots, starting from the most left robot, and following the sequence of the number in green circle. Red lines mean the two robots will swap the transmit and receive mode after that ranging.

B. System Model and Problem Formulation

Fig. 2. This relative state is the core problem of this paper and needs to be estimated based on the inputs and measurements.

The kinematic model of the swarm of aerial robots can be derived based on Newton formula, and the model takes the transformed velocity and yaw rate as the inputs directly. The continuous model $f(\mathbf{X}_{ij})$ is given by [17]

$$\dot{\mathbf{X}}_{ij} = f(\mathbf{X}_{ij}) = \begin{bmatrix} R(\psi_{ij})\mathbf{v}_j - \mathbf{v}_i - Sr_i\mathbf{p}_{ij} \\ r_j - r_i \end{bmatrix} \quad (3)$$

where $\mathbf{v}_i = [v_i^x, v_i^y]^T$ and $\mathbf{v}_j = [v_j^x, v_j^y]^T$ represent the 2-axis horizontal velocity of two robots; $\mathbf{p}_{ij} = [x_{ij}, y_{ij}]^T$ is a part of relative state \mathbf{X}_{ij} meaning 2-axis relative position. $R(\cdot)$ is the rotation function from j^{th} horizontal frame to i^{th} horizontal frame, and S is a skew-symmetric matrix. They are defined as

$$R(\cdot) = \begin{bmatrix} c(\cdot) & -s(\cdot) \\ s(\cdot) & c(\cdot) \end{bmatrix}, \quad S = \begin{bmatrix} 0 & -1 \\ 1 & 0 \end{bmatrix}. \quad (4)$$

Overall, the problem is to estimate the relative state \mathbf{X}_{ij} based on the relative motion model Eq. (3), inputs of \mathbf{U}_{ij} , and measurements of h_i , h_j and d_{ij} . Since the height measurement is accurate, it is used directly for relative position augmentation and height control.

III. RELATIVE LOCALIZATION AND OBSERVABILITY

This section will give details of the relative state estimation method, following by an observability analysis. EKF is used here for estimation because it is efficient compared to other filters such as the particle filter, and it is more apt to micro robots with limited computation power. Lie derivatives are employed to analyze the observability of the system.

A. EKF Filter for Relative Localization

Based on the standard EKF, its application to the discrete model $F(\hat{\mathbf{X}}_k, \mathbf{U}_k)$ of Eq. (3) can be derived as follows.

$$\begin{aligned} \hat{\mathbf{X}}_{k+1|k} &= F(\hat{\mathbf{X}}_k, \mathbf{U}_k) = \hat{\mathbf{X}}_k + \dot{\mathbf{X}}_k \Delta t, \\ \mathbf{P}_{k+1|k} &= \mathbf{A}_k \mathbf{P}_{k|k} \mathbf{A}_k^T + \mathbf{B}_k \mathbf{Q}_k \mathbf{B}_k^T \end{aligned} \quad (5)$$

where Δt is the interval time of updating the Kalman filter, the predicted state is represented by $\hat{\mathbf{X}}_{k+1|k}$, and $\hat{\mathbf{X}}_{k|k}$ is the estimated state at time step k . Furthermore, the first equation in Eq. (5) shows the prediction result using the nonlinear model of Eq. (3). The second equation denotes the update of error covariance \mathbf{P} caused by the prediction step and input noise covariance \mathbf{Q} . To update \mathbf{P} , the state Jacobian matrix \mathbf{A} and input Jacobian matrix \mathbf{B} are calculated as follows.

$$\begin{aligned} \mathbf{A} &= \frac{\partial F}{\partial \mathbf{X}} = \begin{bmatrix} 1 & r_i \Delta t & (-s(\psi_{ij})v_j^x - c(\psi_{ij})v_j^y) \Delta t \\ -r_i \Delta t & 1 & (c(\psi_{ij})v_j^x - s(\psi_{ij})v_j^y) \Delta t \\ 0 & 0 & 1 \end{bmatrix} \\ \mathbf{B} &= \frac{\partial F}{\partial \mathbf{U}} = \begin{bmatrix} -1 & 0 & y_{ij} & c(\psi_{ij}) & -s(\psi_{ij}) & 0 \\ 0 & -1 & -x_{ij} & s(\psi_{ij}) & c(\psi_{ij}) & 0 \\ 0 & 0 & -1 & 0 & 0 & 1 \end{bmatrix} \end{aligned} \quad (6)$$

After the prediction update, the Kalman filter will fuse the predicted state with the observation of the distance between two robots, represented by

$$z = h(\mathbf{X}_{ij}) = \sqrt{x_{ij}^2 + y_{ij}^2 + (h_j - h_i)^2}. \quad (7)$$

Therefore, the Jacobian matrix of observation is

$$\mathbf{H} = \frac{\partial h}{\partial \mathbf{X}} = [x_{ij}/z, y_{ij}/z, 0]. \quad (8)$$

The rest of the Kalman filter process is shown as follows.

$$\begin{aligned} \mathbf{K}_k &= \mathbf{P}_{k|k-1} \mathbf{H}_k^T (\mathbf{H}_k \mathbf{P}_{k|k-1} \mathbf{H}_k^T + \mathbf{R}_k)^{-1}, \\ \hat{\mathbf{X}}_k &= \hat{\mathbf{X}}_{k|k-1} + \mathbf{K}_k (z_k - \mathbf{H}_k \hat{\mathbf{x}}_{k|k-1}), \\ \mathbf{P}_k &= (\mathbf{I} - \mathbf{K}_k \mathbf{H}_k) \mathbf{P}_{k|k-1} \end{aligned} \quad (9)$$

where \mathbf{K} is the Kalman gain. Here, both \mathbf{Q} and \mathbf{R} are noise covariance parameters and can be formulated as diagonal matrices denoted by $\mathbf{Q} = \text{diag}([q_v^2, q_v^2, q_r^2, q_v^2, q_v^2, q_r^2])$ and $\mathbf{R} = \text{diag}([r_d^2])$. q_v , q_r and r_d denote the deviation of the velocity, yaw rate and distance measurements.

B. Observability Analysis

From [20], a local weak observability analysis can be performed with model (3) and observation (7). The observability matrix \mathbf{O} is composed by different orders of Lie derivatives.

$$\mathbf{O} = \begin{bmatrix} \nabla \mathcal{L}_f^0 h \\ \nabla \mathcal{L}_f^1 h \\ \nabla \mathcal{L}_f^2 h \end{bmatrix} = \begin{bmatrix} (\partial \mathcal{L}_f^0 h) / (\partial \mathbf{X}) \\ (\partial \mathcal{L}_f^1 h) / (\partial \mathbf{X}) \\ (\partial \mathcal{L}_f^2 h) / (\partial \mathbf{X}) \end{bmatrix} \quad (10)$$

where $\mathcal{L}_f h$ is the Lie derivative of the model function f , and $\nabla \mathcal{L}_f h$ is the differential operator of the Lie derivatives. For simplicity, the power format $\mathbf{p}_{ij}^T \mathbf{p}_{ij} / 2$ is taken as $h(\mathbf{X}_{ij})$ in this subsection. Substitute system model and observation function, and get

$$\begin{aligned} \mathcal{L}_f^0 h &= h(\mathbf{X}_{ij}) = \mathbf{p}_{ij}^T \mathbf{p}_{ij} / 2 \\ \nabla \mathcal{L}_f^0 h &= [\mathbf{p}_{ij}^T \quad 0] \\ \mathcal{L}_f^1 h &= \nabla \mathcal{L}_f^0 h \cdot f = \mathbf{p}_{ij}^T (R(\psi_{ij})\mathbf{v}_j - \mathbf{v}_i - Sr_i\mathbf{p}_{ij}) \\ \nabla \mathcal{L}_f^1 h &= [(R\mathbf{v}_j - \mathbf{v}_i)^T \quad \mathbf{p}_{ij}^T R(\psi_{ij})S\mathbf{v}_j] \\ \mathcal{L}_f^2 h &= \nabla \mathcal{L}_f^1 h \cdot f = \mathbf{v}_j^T \mathbf{v}_j - 2\mathbf{v}_i^T R\mathbf{v}_j + \mathbf{v}_i^T \mathbf{v}_i + \mathbf{v}_i^T Sr_i\mathbf{p}_{ij} \\ &\quad + \mathbf{p}_{ij}^T R(\psi_{ij})S\mathbf{v}_j r_i \\ \nabla \mathcal{L}_f^2 h &= [\mathbf{v}_i^T Sr_i + r_j \mathbf{v}_j^T S^T R^T \quad -2\mathbf{v}_i^T R S \mathbf{v}_j - \mathbf{p}_{ij}^T R \mathbf{v}_j r_j]^T \end{aligned} \quad (11)$$

According to the local weak observability theory, the system is observable only if observability matrix \mathbf{O} is full rank. In other words, the determinant of the matrix in Eq. (10) should be non-zero. The determinant is calculated as

$$\begin{aligned} |\mathbf{O}| &= -\mathbf{p}_{ij}^T R S \mathbf{v}_j (\mathbf{v}_i^T Sr_i + r_j \mathbf{v}_j^T S^T R^T) S \mathbf{p}_{ij} \\ &\quad - (2\mathbf{v}_i^T R S \mathbf{v}_j + \mathbf{p}_{ij}^T R \mathbf{v}_j r_j) (-\mathbf{v}_i^T + \mathbf{v}_j^T R^T) S \mathbf{p}_{ij} \end{aligned} \quad (12)$$

Although it is difficult to get the full analytical solution of $|\mathbf{O}| \neq 0$ from Eq. (12), we can extract some intuitive and practical unobservable conditions. For example, $|\mathbf{O}|$ tends to be zero when \mathbf{p}_{ij} is close to zero. This means compact movements of this multi-robot system will cause lower estimation accuracy. Also, \mathbf{v}_j cannot be zero, simply

because the i^{th} robot cannot find out the heading of j^{th} robot if j^{th} robot is not moving. However, v_i could be zero in Eq. (12), because the relative state is represented in the body frame of robot i^{th} and it knows its own heading, even if it is static.

Another important unobservable condition is formation behavior of multiple robots, in which the relative velocity $-\mathbf{v}_i^T + \mathbf{v}_j^T R^T$ is zero. This will cause the second term of Eq. (12) to be zero, and the first term is also zero when yaw rates of both robots remain zero. This seems a seriously limiting condition, as this is exactly what happens in most formation flights. The influence of these unobservable conditions will be discussed in the simulation and experiments.

IV. SIMULATION

In this section, the relative localization method for multiple robots is validated by means of simulation results. These have been implemented using Python. The results show the estimation accuracy, convergence performance such as time usage, and estimation efficiency in unobservable conditions.

A. Localization Performance

In this simulation, the relative state between two robots is estimated and compared to the ground-truth relative position and yaw to verify the localization accuracy. This simulation is configured with time interval $dt=0.01s$ and maximum moving velocity of 1m/s. The settings of the simulation are: input noise deviation of 0.25m/s and 0.01rad/s, and a distance measurement deviation 0.1m. The initial estimated states are set to zero, while the ground-truth initial states are set randomly and uniformly in a range of $[-3,3]m$ and $[-1,1]rad$. The parameters of the relative EKF are set to be $\mathbf{Q} = \text{diag}([0.25^2, 0.25^2, 0.4^2, 0.25^2, 0.25^2, 0.4^2])$, $\mathbf{R} = 0.1^2$, and $\mathbf{P} = \text{diag}([10, 10, 0.1])$.

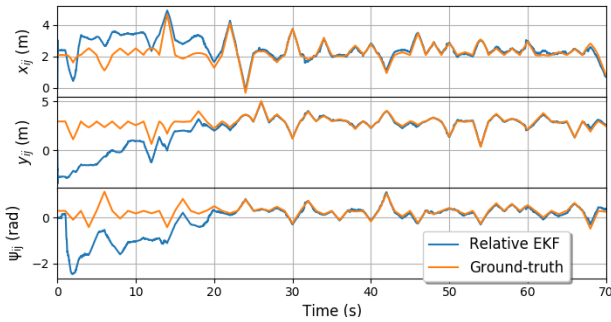


Fig. 4. Simulation results of the relative state estimation between two robots on x_{ij} , y_{ij} , and ψ_{ij} . Both robots are randomly initialized at unknown position and yaw, and they are 2 meter far away each other. Then each robot flies a start-up procedure with 2-second periodic random settings of velocity and yaw rate (1-sec positive velocity and 1-sec negative velocity to guarantee that it flies within 1 meter and not collide with other robots). The orange line represents the ground-truth relative states, while the blue line means the relative states estimated by EKF.

The robots are made to perform random maneuvers at start-up. These allow the filter to converge. Relative localization results are shown in Fig. 4, where we can see that the relative position and yaw approximate the ground-truth

after random flight. As further shown in Fig. 5, this localization with random flight initialization is robust to arbitrary unknown initial states of all robots, and the accuracy will keep high after the convergence. In addition, the localization is stable even if the velocity and yaw rate are time-varying among all robots.

B. Convergence Time

An interesting parameter for our purposes is the expected time to convergence of the estimation. This will dictate how long an initialization maneuver should be before the filter has converged and the swarm can begin to perform coordinated tasks. To evaluate this, we extracted the performance over a set of 50 simulations. These tests are conducted with different random initial position and yaw for each robot, and the inputs of velocity and yaw rate are also randomized.

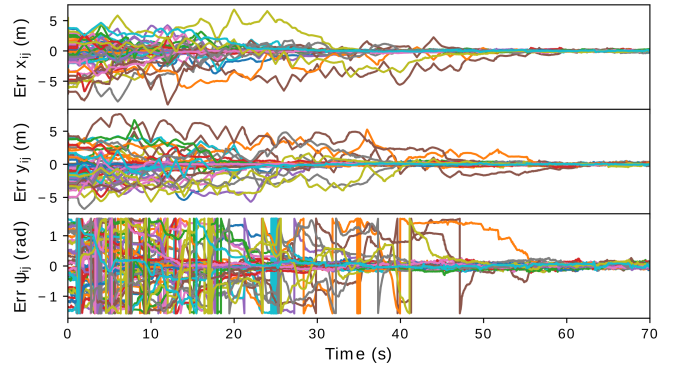


Fig. 5. Estimation error of 3 dimensional relative states from 50 tests with different configurations. Each line with different color means different estimation test in three states of x_{ij} , y_{ij} , and ψ_{ij} . All errors are calculated by comparing the estimated states with the ground-truth.

The results are shown in Fig. 5, which shows the relative estimation error. In all 50 different random tests, the errors of three relative states x_{ij} , y_{ij} , and ψ_{ij} tend to be zero after a certain amount of seconds of random flight. The average convergence time is within 20 seconds, while some tests have larger convergence times, between 20 and 60 seconds, potentially due to inactive inputs, the initialization being further away from the true initial state, or unobservability-inducing flight behaviours. Overall, the short average convergence time and accurate localization are good enough for multi-robot control.

C. Unobservable maneuvers

In section III-B, we analytically showed that some flight conditions are unobservable. This subsection will study the influence of unobservable flight behaviour on the relative localization *after* estimation convergence. Two situations that lead to $|\mathbf{O}| = 0$ will be discussed: 1) Formation flight that causes $-\mathbf{v}_i^T + \mathbf{v}_j^T R^T = 0$, and at same time yaw rates of r_i and r_j keep zero; 2) the j^{th} robot has zero velocity, i.e. $\mathbf{v}_j = 0$, where relative yaw ψ_{ij} should be unobservable.

In Fig. 6, relative localization performance with unobservability-inducing control inputs are shown. By comparing the red and blue boxes, the influences of formation

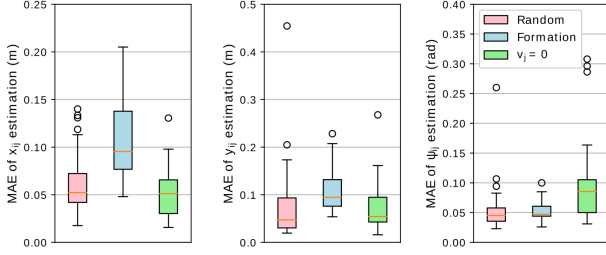


Fig. 6. Error distribution of 3 dimensional relative estimation in different unobservable situations. For each situation, these mean absolute errors (MAE) are obtained from 50 different tests, during the 20 seconds after the estimation convergence. Boxes of red, blue, and green color represent the normal random flight, formation flight, and zero velocity of the j^{th} robot, respectively.

flight have: 1) an increase of estimation errors on all relative states; 2) the relative estimation is still stable with position error less than 0.2m. This can be explained because once the estimation is not correct, robots will slightly deviate from their role in the formation (in terms of velocity, position), which in turn makes the system observable again. Hence, it seems that the unobservability problem is a self-stabilizing phenomenon that operates within acceptable precision bounds. In the case that the robot to be localized has zero velocity, the relative yaw estimation has a larger error compared to the normal random flight, which can be seen from the green box. However, as indicated in section III-B, the relative position of x_{ij} and y_{ij} are still observable. Therefore, the green boxes have similar estimation error with the red boxes in axes of x_{ij} and y_{ij} .

V. REAL-WORLD EXPERIMENTAL RESULTS

Using simulations, we have shown that the filter is capable of converging to correct estimates by means of randomized flight maneuvers, after which it can be effectively used for cooperative flight. This section presents an experimental setup in order to further illustrate the relative estimation efficiency in a real-world multi robot system. The test scenarios consist of formation flight and autonomous flight based on the monocular camera on the lead robot.

A. Hardware Setup

The swarm of aerial robot system consists of 5 commercial quadrotors of Crazyflie2. Each quadrotor is equipped with a 3-axis accelerometer, 3-axis gyroscope, VL53L1x height sensor, PMW3901 optical flow sensor, and DWM1000 ultra wide-band sensor. The flow sensor can provide velocity at 100Hz, while the distance measurement frequency of UWB relies on the number of robot to be discussed later. The processor is an STM32F4 running at 168MHz, on which both relative estimation and control are running.

A motion capture system optiTrack is used for tracking the ground-truth position and yaw of each robot. The optiTrack data is only used for post-processing to validate the relative estimation performance, and has not been used for any other purpose.

B. Data Processing and Communication Performance

The raw ranging measurements from UWB can have outliers and unknown bias. Thus, a median filter is applied to reject the outliers, and a bias function is predetermined by data fitting based on the ground-truth distance from optiTrack.

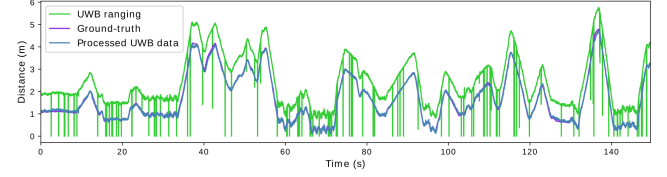


Fig. 7. UWB measurements and data processing. The green line shows the original distance measurements with large outliers. The blue line shows the outlier-rejected and bias compensated distance data. And the purple line is the ground-truth distance from optiTrack.

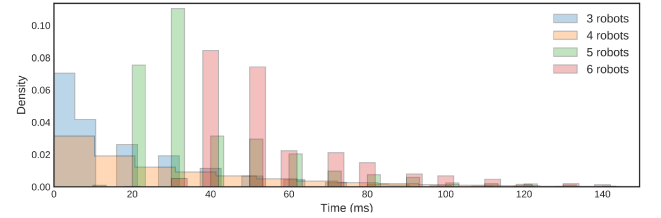


Fig. 8. The distribution of ranging and communication frequency between each two robots with the increase of the number of robots.

The linear bias fitting function is related to the distance, represented by $bias = 0.072 * dist + 0.62$. By median filtering and subtracting the bias, the processed distance is accurate and approximates the ground-truth distance as shown in Fig. 7. Fig. 8 shows the frequency of the proposed communication in section II-A. As seen from Fig. 8, the frequency decreases with the increase of the number of robots, but it is still 20Hz for 6 robots, and much better than 16Hz with 3 robots in [17].

C. Formation Flight

First, the real-world relative estimation performance is shown Fig. 9, which indicates the short convergence time and accurate estimation on real robots. System with more number of robots has longer convergence time due to the lower frequency of communication and EKF update.

Then a formation flight of 5 robots is conducted based on the relative states. In formation flight, each robot has a reference relative state \tilde{p}_{ij} , and $j = 1$ in this test. The state error is denoted by $e_{ij} = \tilde{p}_{ij} - \hat{p}_{ij}$. Therefore, PID-based formation control inputs are

$$v_i = k_p * e_{ij} + k_d * \dot{e}_{ij} + k_i * \int e_{ij} dt \quad (13)$$

Fig. 10 shows that the robot team can achieve a formation flight after a random flight for relative localization. Five parts with dense trajectories represent different initial random position of each robot. After the random flight, they form a Olympic-symbol-like pattern formation shown by the polygon

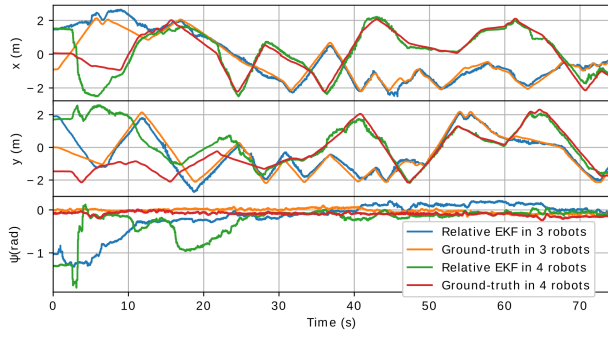


Fig. 9. Real-world relative localization in 3-robot and 4-robot systems respectively. Here, x , y and z denote the absolute XY position and yaw of the 2nd robot, calculated by the relative EKF from the 1st robot, and compared with ground-truth from optiTrack.

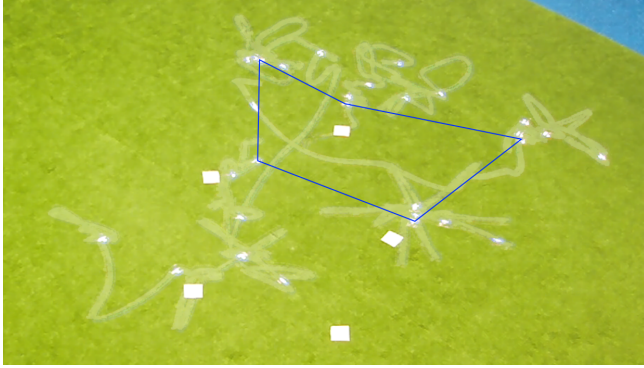


Fig. 10. Pattern formation trajectories of 5 robots over time. Polygon means the final pattern formation similar to Olympic Flag. More details can be found in the video link in the first page.

in Fig. 10, and this formation is kept well even if all robots hover in the air.

D. Autonomous Coordinate Visual Task

This part further explores the proposed localization ability for autonomous task by multiple heterogeneous flying robots. The first, leading robot is equipped with a camera. This enables it to detect the four points of the window based on a color filtering and histogram method shown in Fig. 11, and controls its two-axis velocity to move through the center of the window indefinitely. At the same time, another robot coordinates with the lead robot in order to fly through the window. As seen in Fig. 11, the follower robot has stable coordinate behaviour with respect to the lead robot, and flies through the window without extra camera detection based only on relative localization. These follower robots could in a real scenario be equipped with different gas sensors (one robot with a CO-sensor, the other with a CH₄ sensor, etc.).

VI. CONCLUSIONS

This paper proposes a relative localization method and applies it to a swarm of micro flying robots. These multiple robots only require onboard sensing information, without any external system or magnetometer. The general multi-robot kinematic model and observability analysis are provided. The



Fig. 11. Experimental results of coordinated leader-follower flight through a window. Two drones connected with a line are captured at a specific time, and the one with arrow means the leader. Only the leader drone is equipped with monocular camera shown in the left-up corner, and the follower robot coordinates based on the estimated relative position. The window detection results and its four points are shown in the right-down corner.

relative localization speed and accuracy are verified in both simulation and experimental results. The simulation and real-world experiments show that unobservable conditions of this type of relative localization actually lead to a self-stabilizing system with acceptable accuracy. Finally, multi-robot tasks are tested in this swarm system, including formation flight and coordinated window fly-through of multiple robots with only onboard resources.

Future work could include the development of an optimal initialization for this relative state estimation, in order to reduce the convergence time. Also, a new framework for the communication protocol can improve the scalability properties of the swarm, since currently it is limited by the ranging frequency between the robots.

REFERENCES

- [1] Q. Lindsey, D. Mellinger, and V. Kumar, "Construction of cubic structures with quadrotor teams," *Proc. Robotics: Science & Systems VII*, 2011.
- [2] R. Ritz, M. W. Müller, M. Hehn, and R. D'Andrea, "Cooperative quadcopter ball throwing and catching," in *2012 IEEE/RSJ International Conference on Intelligent Robots and Systems*. IEEE, 2012, pp. 4972–4978.
- [3] M. Gassner, T. Cieslewski, and D. Scaramuzza, "Dynamic collaboration without communication: Vision-based cable-suspended load transport with two quadrotors," in *2017 IEEE International Conference on Robotics and Automation (ICRA)*. IEEE, 2017, pp. 5196–5202.
- [4] M. A. Estrada, S. Mintchev, D. L. Christensen, M. R. Cutkosky, and D. Floreano, "Forceful manipulation with micro air vehicles," *Science Robotics*, vol. 3, no. 23, p. eaau6903, 2018.
- [5] K. McGuire, C. De Wagter, K. Tuyls, H. Kappen, and G. de Croon, "Minimal navigation solution for a swarm of tiny flying robots to explore an unknown environment," *Science Robotics*, vol. 4, no. 35, p. eaaw9710, 2019.
- [6] A. Kushleyev, D. Mellinger, C. Powers, and V. Kumar, "Towards a swarm of agile micro quadrotors," *Autonomous Robots*, vol. 35, no. 4, pp. 287–300, 2013.
- [7] J. A. Preiss, W. Honig, G. S. Sukhatme, and N. Ayanian, "Crazyswarm: A large nano-quadcopter swarm," in *2017 IEEE International Conference on Robotics and Automation (ICRA)*. IEEE, 2017, pp. 3299–3304.
- [8] G. Vásárhelyi, C. Virágh, G. Somorjai, T. Nepusz, A. E. Eiben, and T. Vicsek, "Optimized flocking of autonomous drones in confined environments," *Science Robotics*, vol. 3, no. 20, p. eaat3536, 2018.
- [9] M. Hamer and R. DAndrea, "Self-calibrating ultra-wideband network supporting multi-robot localization," *IEEE Access*, vol. 6, pp. 22 292–22 304, 2018.

- [10] J. Faigl, T. Krajník, J. Chudoba, L. Přeucil, and M. Saska, "Low-cost embedded system for relative localization in robotic swarms," in *2013 IEEE International Conference on Robotics and Automation*. IEEE, 2013, pp. 993–998.
- [11] M. Saska, T. Baca, J. Thomas, J. Chudoba, L. Preucil, T. Krajník, J. Faigl, G. Loianno, and V. Kumar, "System for deployment of groups of unmanned micro aerial vehicles in gps-denied environments using onboard visual relative localization," *Autonomous Robots*, vol. 41, no. 4, pp. 919–944, 2017.
- [12] A. Carrio, S. Vemprala, A. Ripoll, S. Saripalli, and P. Campoy, "Drone detection using depth maps," in *2018 IEEE/RSJ International Conference on Intelligent Robots and Systems (IROS)*. IEEE, 2018, pp. 1034–1037.
- [13] A. Weinstein, A. Cho, G. Loianno, and V. Kumar, "Visual inertial odometry swarm: An autonomous swarm of vision-based quadrotors," *IEEE Robotics and Automation Letters*, vol. 3, no. 3, pp. 1801–1807, 2018.
- [14] M. Coppola, K. N. McGuire, K. Y. Scheper, and G. C. de Croon, "On-board communication-based relative localization for collision avoidance in micro air vehicle teams," *Autonomous robots*, vol. 42, no. 8, pp. 1787–1805, 2018.
- [15] K. Guo, Z. Qiu, W. Meng, L. Xie, and R. Teo, "Ultra-wideband based cooperative relative localization algorithm and experiments for multiple unmanned aerial vehicles in gps denied environments," *International Journal of Micro Air Vehicles*, vol. 9, no. 3, pp. 169–186, 2017.
- [16] T. Nguyen, Z. Qiu, T. H. Nguyen, M. Cao, and L. Xie, "Distance-based cooperative relative localization for leader-following control of mavs," *IEEE Robotics and Automation Letters*, vol. 4, no. 4, pp. 3641–3648, Oct 2019.
- [17] S. van der Helm, M. Coppola, K. N. McGuire, and G. C. de Croon, "On-board range-based relative localization for micro air vehicles in indoor leader-follower flight," *Autonomous Robots*, pp. 1–27, 2019.
- [18] M. Greiff, "Modelling and control of the crazyflie quadrotor for aggressive and autonomous flight by optical flow driven state estimation," *MSc. Thesis*, 2017.
- [19] M. W. Mueller, M. Hamer, and R. D'Andrea, "Fusing ultra-wideband range measurements with accelerometers and rate gyroscopes for quadcopter state estimation," in *2015 IEEE International Conference on Robotics and Automation (ICRA)*. IEEE, 2015, pp. 1730–1736.
- [20] R. Hermann and A. Krener, "Nonlinear controllability and observability," *IEEE Transactions on automatic control*, vol. 22, no. 5, pp. 728–740, 1977.